AFRL-RD-PS-
TR-2017-0055

DURABILITY TESTING OF ADDITIVELY MANUFACTURED HIGH POWER MICROWAVE STRUCTURES

Nicholas Jordan

The Regents of The University of Michigan
3003 South State Street
Ann Arbor, MI 48109-1274

29 October 2017

Final Report

AIR FORCE RESEARCH LABORATORY
Directed Energy Directorate
3550 Aberdeen Ave SE
AIR FORCE MATERIEL COMMAND
KIRTLAND AIR FORCE BASE, NM 87117-5776

NOTICE AND SIGNATURE PAGE

Using Government drawings, specifications, or other data included in this document for any purpose other than Government procurement does not in any way obligate the U.S. Government. The fact that the Government formulated or supplied the drawings, specifications, or other data does not license the holder or any other person or corporation; or convey any rights or permission to manufacture, use, or sell any patented invention that may relate to them.

This report was cleared for public release by the Air Force Research Laboratory RD Public Affairs Office and is available to the general public, including foreign nationals. Copies may be obtained from the Defense Technical Information Center (DTIC) (http://www.dtic.mil).

AFRL-RD-PS-TR-2017-0055 HAS BEEN REVIEWED AND IS APPROVED FOR PUBLICATION IN ACCORDANCE WITH ASSIGNED DISTRIBUTION STATEMENT.

HOFF.BRAD.WINSTON.1188079721 Digitally signed by HOFF.BRAD.WINSTON.1188079721 Date: 2018.02.16 13:53:30 -07'00'

BRAD HOFF, DR-III
Program Manager

Stephen Langdon

STEPHEN LANGDON, DR-III
Chief, HPEM Technologies Division

This report is published in the interest of scientific and technical information exchange, and its publication does not constitute the Government's approval or disapproval of its ideas or findings.

20REPORT DOCUMENTATION PAGE

Form Approved
OMB No. 0704-0188

1. REPORT DATE *(DD-MM-YYYY)*	**2. REPORT TYPE**	**3. DATES COVERED** *(From - To)*
29-10-2017	Final Report	31-05-2016 – 29-09-2017

4. TITLE AND SUBTITLE

Durability Testing of Additively Manufactured High Power Microwave Structures

5a. CONTRACT NUMBER

5b. GRANT NUMBER
FA9451-16-1-0050

5c. PROGRAM ELEMENT NUMBER
62605F

6. AUTHOR(S)

Nicholas Jordan

5d. PROJECT NUMBER
4867WTAA

5e. TASK NUMBER
EF127845

5f. WORK UNIT NUMBER
D09K

7. PERFORMING ORGANIZATION NAME(S) AND ADDRESS(ES)

The Regents of The University of Michigan
3003 South State Street
Ann Arbor, MI 48109-1274

8. PERFORMING ORGANIZATION REPORT NUMBER

9. SPONSORING / MONITORING AGENCY NAME(S) AND ADDRESS(ES)

Air Force Research Laboratory
3550 Aberdeen Avenue SE
Kirtland AFB, NM 87117-5776

10. SPONSOR/MONITOR'S ACRONYM(S)

AFRL/RDHP

11. SPONSOR/MONITOR'S REPORT NUMBER(S)

AFRL-RD-PS-TR-2017-0055

12. DISTRIBUTION / AVAILABILITY STATEMENT

APPROVED FOR PUBLIC RELEASE: DISTRIBUTION IS UNLIMITED

13. SUPPLEMENTARY NOTES

"Government Purpose Rights"

14. ABSTRACT

Anode structures for a relativistic planar magnetron were 3D printed from a photopolymer using a stereolithography printing process. One anode was electroplated with copper, whereas the other was thermal-sprayed with copper. The performance and durability of these structures were evaluated in comparison to a solid aluminum anode fabricated via conventional machining. The experimental parameters were: cathode voltages between -150 and -300 kV, voltage pulselengths of 200-600 ns, axial magnetic fields of 0.13-0.31 T, peak anode currents from 1-7 kA, and a base operating pressure of 9×10^{-6} torr. The 3D printed anodes demonstrated comparable microwave performance to the aluminum anode, generating microwave powers in excess of 150 MW. After 100 shots on each structure, neither anode showed any signs of operationally-induced damage. A subsequent experiment has been designed and constructed to evaluate durability over longer time-periods.

15. SUBJECT TERMS

Additive manufacturing, 3D printing, high power microwaves, relativistic magnetron, recirculating planar magnetron

16. SECURITY CLASSIFICATION OF:			**17. LIMITATION OF ABSTRACT**	**18. NUMBER OF PAGES**	**19a. NAME OF RESPONSIBLE PERSON**
a. REPORT	**b. ABSTRACT**	**c. THIS PAGE**			Brad Hoff
Unclassified	Unclassified	Unclassified	SAR	26	**19b. TELEPHONE NUMBER** *(include area code)*

Standard Form 298 (Rev. 8-98)
Prescribed by ANSI Std. 239.18

TABLE OF CONTENTS

Section **Page**

List of Figures

Figure **Page**

LIST OF TABLES

Table **Page**

1.0 SUMMARY

This report presents efforts to test additively manufactured components in high power microwave (HPM) systems. Performance, durability, manufacturing tolerances and outgassing are evaluated. Additively manufactured components were successfully fielded for the first time in a relativistic crossed-field device. Anode structures for a relativistic planar magnetron were 3D printed from a photopolymer using a stereolithography (SLA) printing process. One anode was electroplated with copper, whereas the other was thermal-sprayed with copper. The coating thickness at the vane tips was approximately 0.18 mm and 0.23 mm, respectively. The performance and durability of these structures were evaluated in comparison to a solid aluminum anode fabricated via conventional machining. The experimental parameters were: cathode voltages between -150 and -300 kV, voltage pulselengths of 200 to 600 ns, axial magnetic fields of 0.13 T to 0.31 T, peak anode currents from 1 to 7 kA and a base operating pressure of $9x10^{-6}$ torr. The 3D printed anodes demonstrated comparable microwave performance to the aluminum anode, generating microwave powers in excess of 150 MW, with an average instantaneous peak total efficiency of 27% $\pm$ 10%. After 100 shots on each structure, neither anode showed any signs of operationally-induced damage. The anodes did, however, have a higher rate of post-shot outgassing, emitting 32% and 23% more CO_2 per shot, respectively. A subsequent experiment has been designed and constructed to evaluate durability over longer time-periods.

2.0 INTRODUCTION

HPM sources serve a number of important applications in defense, industrial and scientific fields. These applications include radar, materials processing and counter-electronics [1-3]. For some applications, source mobility is desirable. Unfortunately, many HPM sources can be massive enough that incorporating these devices into mobile platforms becomes problematic. Replacing source components with equivalently functional, less massive counterparts is one way to address issues with overall system weight.

An example of this is substitution of metal-coated plastic components for solid metal components, such as demonstrated by Ge, et al. [4]. The L-band relativistic backward wave oscillator (RBWO) of Ge, et al. featured a slow wave structure (SWS) fabricated from a machined plastic base component which was then layered with nickel, copper and then chromium to form a 100 μm metal coating. The metalized plastic SWS was found to perform comparably to a solid stainless steel SWS at power levels approaching 2 GW and pulse durations of 50 ns [4].

It is important to note that in linear beam tubes such as the aforementioned RBWO configuration, the SWS experiences high radio frequency (RF) electric fields, but would not be expected to experience substantial impacting current from the electron beam, thus it is not immediately evident if this technique can be extended to high power crossed field sources. In high power crossed field sources, such as relativistic magnetrons [1-3, 5, 6] and recirculating planar magnetrons (RPM) [7-10], the slow wave structure, which supports the high electric fields associated with the anode-cathode (AK) gap bias as well as the radio frequency wave, also serves as the anode for the electron beam and is directly impacted by a substantial fraction of the electron beam current [1-3, 5-10].

Herein, we investigate the possibility of using a metalized, 3D printed plastic anode structure in a relativistic RPM. We designed the printed anode structures as “drop-in” replacements (i.e. geometric duplicates) of the previously studied aluminum anode structures described by Franzi, et al. [10]. Fabrication of two different 3D printed anode structures, each metalized using a different process, is discussed. RPM performance utilizing each of the printed anodes is compared with recent performance results obtained using the solid aluminum anode structure, as well as with previous results [10].

3.0 METHODS, ASSUMPTIONS, AND PROCEDURES

3.1 Fabrication

The RPM-12a anode (Figure 1a) is composed of two planar cavity arrays joined together by two recirculating bend sections. The four individual pieces are each machined conventionally from a block of aluminum and bolted together at the corners. The RPM-12b and c anodes were fabricated using a SLA printing process, using DSM’s Somos Water Shed XC 11122 photopolymer [11]. This process and polymer were chosen for their high resolution and dense construction, respectively. In previous work, Air Force Research Laboratory (AFRL) has used this particular photopolymer successfully for high voltage applications. The anodes were each printed and coated as a four separate parts, each roughly 10” x 3” x 4.5” and then assembled into the 13.5” wide anode shown in Figure 1b. Commercial SLA printers are capable of fabricating

parts as large as 1 m^3, so the additively manufactured structure could have been fabricated as a single unit, but we chose to match the RPM-12a construction for direct performance comparison. The first set of pieces was coated by Fini-Finish [12] using a multi-stage process. The surface was first coated with a conductive epoxy, then electroplated with copper (Figure 1c) to form the RPM-12b. The second set, RPM-12c, was thermal-sprayed with copper to create a conductive coating (Figure 1d).

The RPM-12a anode, made of Al 6061, weighs 9.4 kg, whereas the uncoated plastic anode weighs 4.0 kg. The electroplated and thermally sprayed coatings add 1.09 and 1.24 kg to the structure, respectively. Measured at the anode vanes, we find the RPM-12b coating to be approximately 0.18 mm thick, whereas the RPM-12c coating is thicker at 0.23 mm. The higher surface roughness of the RPM-12c contributes somewhat to the thicker measurement.

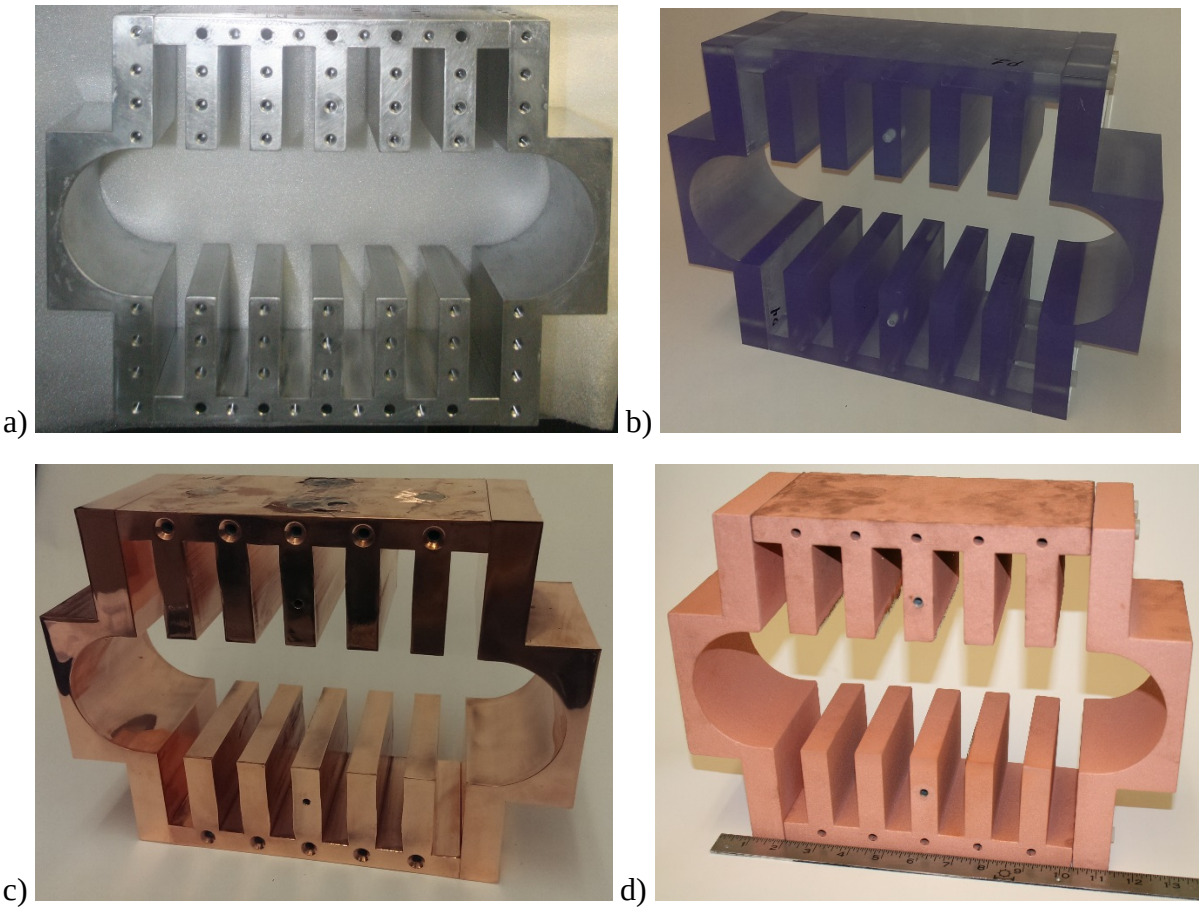

Figure 1: a) RPM-12a Anode, Machined from Aluminum, used as a Baseline for Comparison. b) RPM-12b/c Anode before Coating Process, Composed of Water Shed XC 11122 Photopolymer, which has Similar Properties to ABS or PBT. c) RPM-12b Anode, Electroplated with Copper. Some Damage is Visible on the Top of the Part, as a Result of the Coating Process. d) RPM-12c Anode, Coated Via a Copper Thermal Spray Process. Discoloration on the Top of the Structure is a Result of Post-Test Handling without Gloves

3.2 Challenges and Defects

For these prototypes, there were some notable defects that resulted from the metallization processes. The electroplated structure (RPM-12b) did not have uniform coating thickness, particularly within the anode vanes. As can be seen in Figure 1c, the vanes widen slightly in the back of each cavity. Whereas the outer surfaces were relatively smooth, the interior of each cavity (Figure 2a) did not coat evenly, leading to higher surface roughness and some surface discontinuities. The electroplated structure also suffered from delamination in several places. In these locations, a copper "bubble" would form, usually over 4 cm in diameter and ~1 mm in height. We were initially concerned about trapped gas at the delamination sites and drilled small vent holes in many places to compensate, but many of the copper bubbles were between vanes and inaccessible. When placed under vacuum, the gas did not expand and damage the structure, or create significant virtual leaks. In future work, the variation in coating thickness could be improved by careful design of the electroplating anodes and delamination might be reduced with

better surface preparation and alterations to the anode design to better accommodate the nuances of the electroplating process.

The thermal sprayed structure (RPM-12c) also suffered from variation in coating thickness (Figure 2b). As a line-of-sight process, thermal spray struggles to adequately and uniformly coat small holes or cavities, as well as sharp edges and corners. For the RPM-12c anode, the coating cracked in several places at the edge of the vanes (Figure 2c) and had to be soldered to maintain electrical continuity.

a) 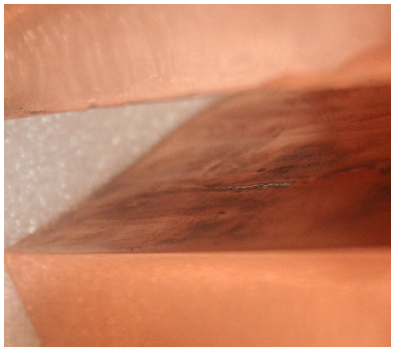 b) 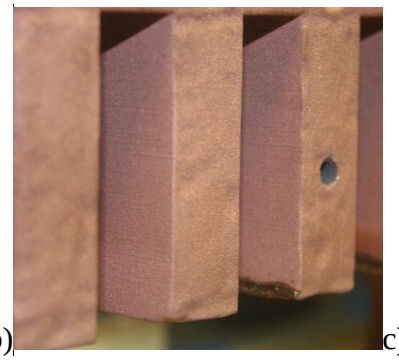 c) 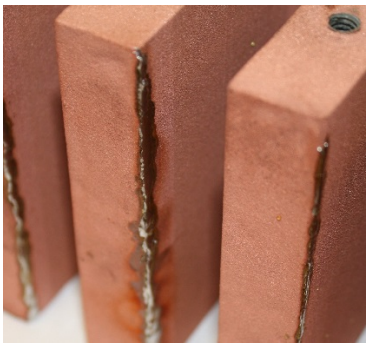

Figure 2: Defects Resulting from the Fabrication Process. Non-Uniform Coating and Thin Cracks (a) were Present Between the Vanes of the Electroplated Structure. The Thermal Spray Process Produced Regions of Uneven Thickness, Resulting in an Orange Peel-Like Appearance (b). The Thermal Spray Process also Resulted in some Cracks Along Vane Edges (c), which we Repaired with Solder Before Testing

3.3 Experimental Configuration

The Michigan Electron Long Beam Accelerator with a ceramic insulator stack (MELBA-C) was the driver for the RPM experiments, providing voltages between -250 and -300 kV for pulselengths of 200 to 600 ns. A pair of pulsed electromagnets are positioned 21.6 cm apart in a pseudo-Helmholtz configuration and centered over the anode region to create a nearly uniform axial magnetic field, which was varied on a per-shot basis from 0.13 to 0.31 T. A #304 stainless steel vacuum chamber housed the magnetron and was operated at base vacuum pressures between 10^{-6} and 10^{-5} torr, as measured by an ion gauge mounted near the inlet to the cryopump, opposite a SRS RGA-200 residual gas analyzer (RGA). A $CuSO_4$ resistive divider sampled the MELBA-C voltage pulse and a Rogowski coil within the vacuum chamber measured the current entering the RPM-12a/b/c.

Figure 3 shows the experimental configuration used for RPM-12a/b/c, with a coaxial extraction system for calibrated power measurements. Microwave power was extracted via two symmetric coaxial waveguides with an inner conductor diameter of 0.75 cm and an outer conductor diameter of 2.5 cm, whose inner conductors were attached directly to the central vane of the anode structure under test. The coaxial transmission line entered a coax-to-waveguide coupler (DFA-650b) and was launched as a $TE_{1,0}$ mode in the waveguide, to be sampled by a directional coupler (-58 dB) and then dissipated in an Ecosorb load. The sampled microwave signals were transmitted to the Faraday cage using two RG-213U N-type cables (5 dB attenuation around 1 GHz) and attenuated by 22 dB using in-line attenuators. The signal was split using a 3 dB power divider to be: 1) directly sampled by a Tek7404 (5 GHz, 10 GS/s per channel) oscilloscope to capture time-dependent frequency information and, 2) rectified by calibrated Agilent 8472B low-barrier Schottky diode microwave detectors, which were connected to a Tek3054 oscilloscope for power measurement.

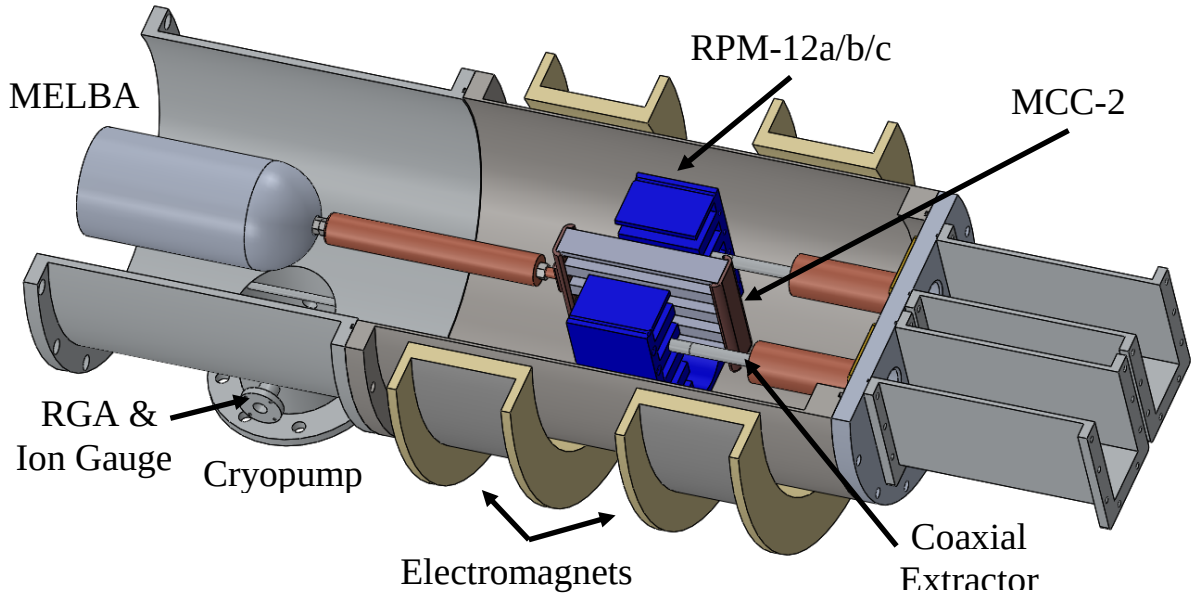

Figure 3: Experimental Configuration for RPM-12a, b and c anode (blue) testing. Power is Axially Extracted via Coaxial Lines and Launched into the Waveguide by Custom Couplers. The Center Conductor of each Coaxial Line Screws into the Anode Structure, Making Electrical Contact at the Surface

The cathode used for all tests was the Mode Control Cathode 2 (MCC-2) [13], which is composed of five hollow, 1.9 x 3.8 cm rectangular tubes, resulting in an AK gap of 2.6 cm. Including the end caps, it was 23 cm in length. To designate an emission region, 1.9 cm^2 velvet squares were attached to the center of the cathode using conductive silver epoxy, whereas the rest of the cathode was coated with several layers of Glyptal insulating paint.

Due to the axial extraction system, an endloss current measurement was not feasible. Endloss measurements were performed using a modification of the setup shown in Figure 3, in which the axial extractors, waveguides and chamber end plate were replaced by a stainless steel electron beam collection plate electrically isolated from the chamber by a 1" Lexan ring. These measurements, in tandem with MAGIC simulations, were used to estimate the endloss current for shots conducted using the configuration shown in Figure 3.

4.0 RESULTS AND DISCUSSION

4.1 Magnetic Field Penetration

We compared the performance of the 3D printed anodes to the baseline case of a 4-piece aluminum anode, the RPM-12a. The differences in anode composition of the RPM-12b/c led to variation in magnetic field diffusion time relative to the RPM-12a. As Figure 4 shows, one of the advantages of using a metallized plastic structure, in conjunction with pulsed electromagnets, is an increase in peak field strength available within the magnetron. Consequently, for the same required magnetic field within the magnetron, a metallized plastic structure will have reduced requirements for its electromagnet. For our experimental setup, the electromagnets have a peak current of 1.1 kA, so the 3D printed structures provided a broader parameter space to explore when identifying operating modes. In the future, it may be possible to create a more spatially

uniform magnetic field within an RPM anode by adding and removing metallic material to optimize the field penetration in simulation. 3D printed structures offer significant flexibility in this regard.

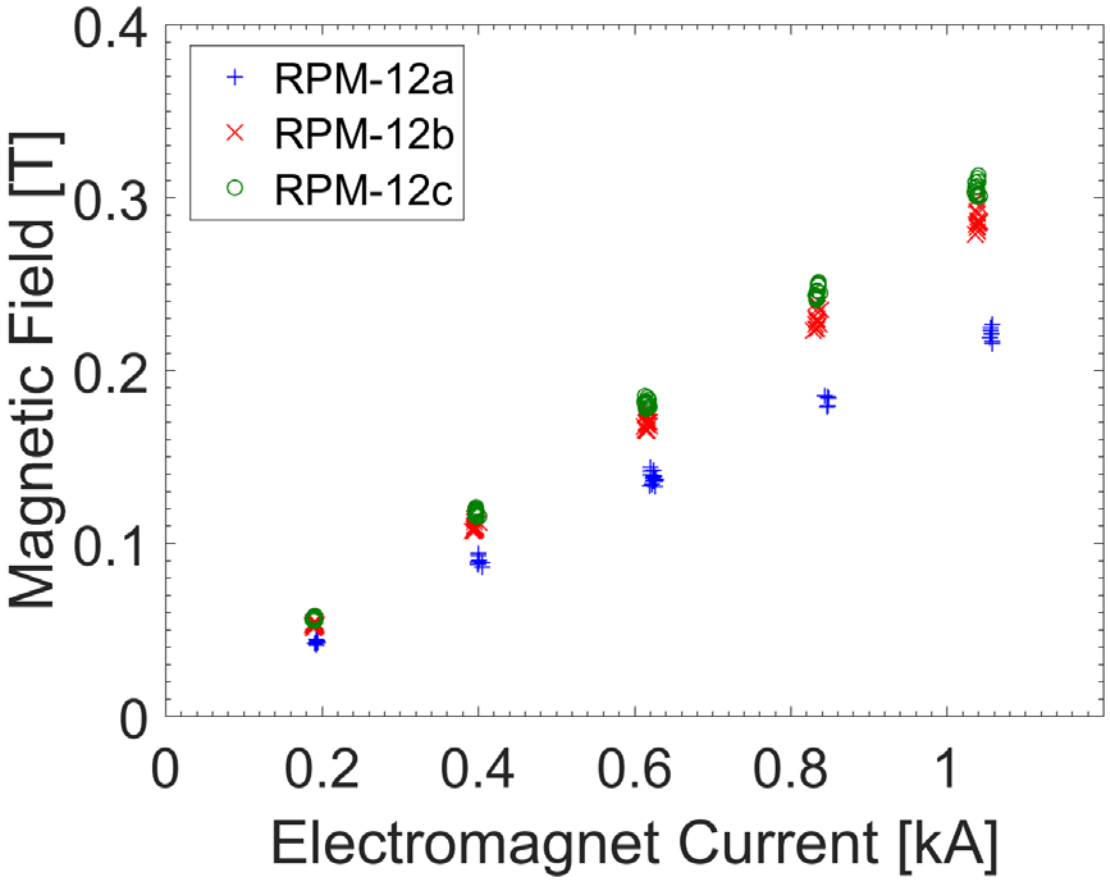

Figure 4: Magnetic Field at the Center Anode Vane as a Function of Input Current, Measured at the Start of Voltage Rise. The 3D Printed Anodes Result in Substantially Higher Fields

4.2 Microwave Performance

Our primary concern for the additively manufactured anodes was to verify that they could withstand repeated use in a HPM device and that their microwave performance was not adversely affected by their construction. Performance and durability characterization involved determination of operating modes and associated frequencies, peak power produced, efficiency of operation and peak anode current experienced.

Figure 5 shows the voltage, current and power waveforms typically observed from the RPM. This particular example was produced by the RPM-12b, but these waveforms were qualitatively very similar for all three anodes. Microwave pulses were approximately 50 to 100 ns in duration, with startup occurring early in the voltage pulse. The magnetic field for the 3D printed anode was varied from 0.13 T to 0.31 T, whereas the range of magnetic fields accessible to the RPM-12a was limited to 0.15 to 0.22 T, as noted in the previous section.

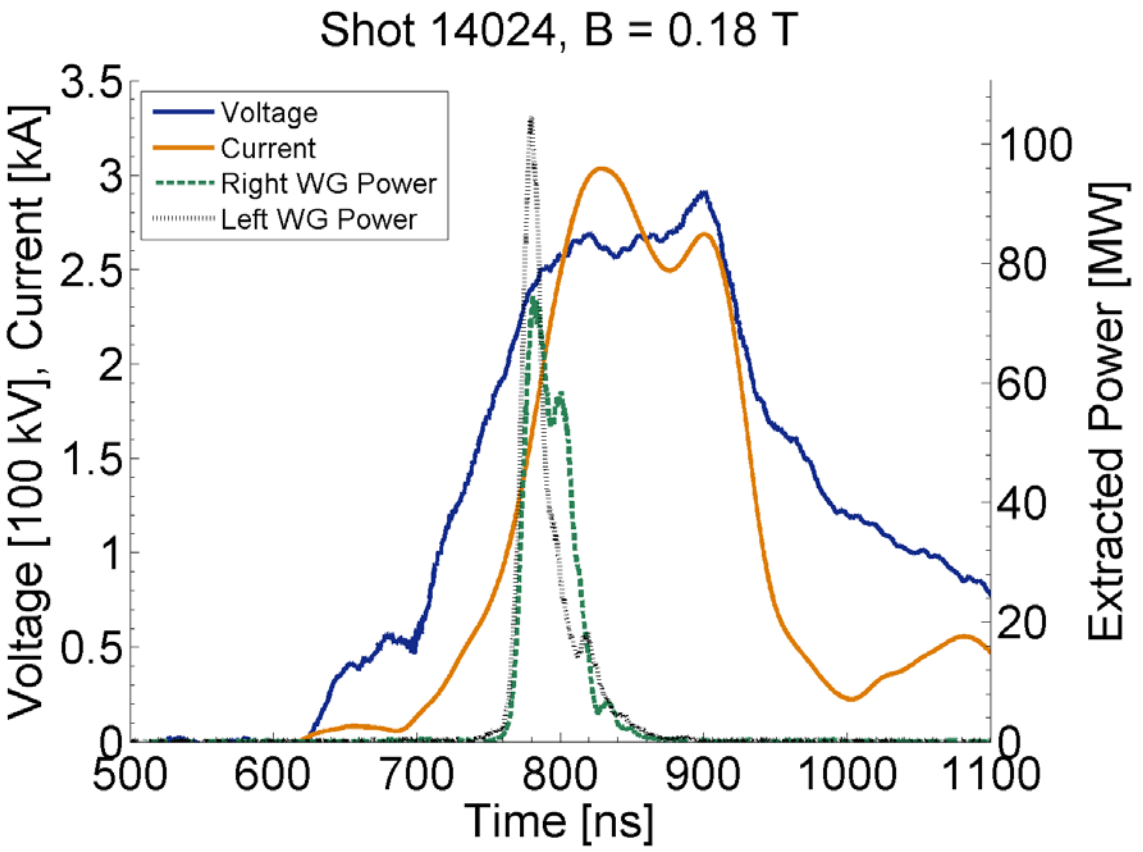

Figure 5: Sample Shot Taken using the RPM-12b. Microwave Pulses were Typically 50-100 ns in Duration and Occurred Early in the Voltage Pulse. Current Runaway at Late Times was well Controlled for all Anodes Tested

As Table 1 shows, the power and efficiency of microwaves produced using the 3D printed anodes was comparable to the solid metal RPM-12a. These data are also in line with previous tests of the RPM-12a [10]. The previous work did not use an optimized magnetic field timing, leading to spatial variations in magnetic field profile. Subsequent improvements in magnetic field uniformity motivated retaking the RPM-12a data. Averages and standard deviations are calculated using only data from shots with a magnetic field between 0.15 and 0.22 T. Applying that filter leaves approximately 45 shots in each data set. Peak total instantaneous efficiencies were determined using the total current (including endloss). Specifically, the efficiency was determined by dividing the peak total output power (sum of both waveguides) by the product of current and voltage at the time of the peak total output power. Therefore, efficiencies in Table 1 are total efficiencies, not electronic efficiencies.

Table 1: In the Range of Axial Magnetic Fields from 0.15-0.22 T, the 3D Printed Anodes Produced Comparable Power and Efficiency to a Traditionally Fabricated Anode. The Uncertainties given are one Standard Deviation

	Average Peak Total Power [MW]	Average Peak Efficiency [%]
RPM-12a	101 +/- 19	20.0 +/- 6.5
RPM-12b	113 +/- 23	25.5 +/- 11.0
RPM-12c	91 +/- 21	28.7 +/- 9.1

Performance characterization also involved identification of the operating frequencies, which could then be related to operating modes predicted from analytical theory and simulation. Fast Fourier Transforms (FFTs) of the RF voltage traces revealed the magnetron primarily operated at approximately either 0.978 GHz or 0.998 GHz. Based on simulations and theory, 0.978 GHz is the $5\pi/6$-mode and 0.998 GHz is the π-mode.

4.3 Durability

By varying the magnetic field, we were able to subject the anodes to a wide range of operating conditions, as shown in Figure 6. As noted previously, the power extraction setup for the current RPM prototype does not allow a direct measurement of endloss current. Consequently, the range of anode currents shown in Figure 6 is based on an estimate of 25% axial current loss (total, from each end of the cathode). For the purposes of this work, the precise value of current striking the anode is not essential. As this figure shows, the RPM-12b & c anodes were subjected to peak anode current over 6 kA and produced peak total power of over 150 MW without sustaining any observable damage or reducion in performance. A typical pulse experienced 2 kA of anode current and produced 100 MW of total peak power. It should be noted that this is the peak anode current, not the current at peak power and is not intended to relate the two quantities in any way. It simply shows the extent of the conditions these anode structures endured over the course of these tests. As a point of comparison, however, total current at peak microwave power was between 1 and 4 kA for all anodes tested.

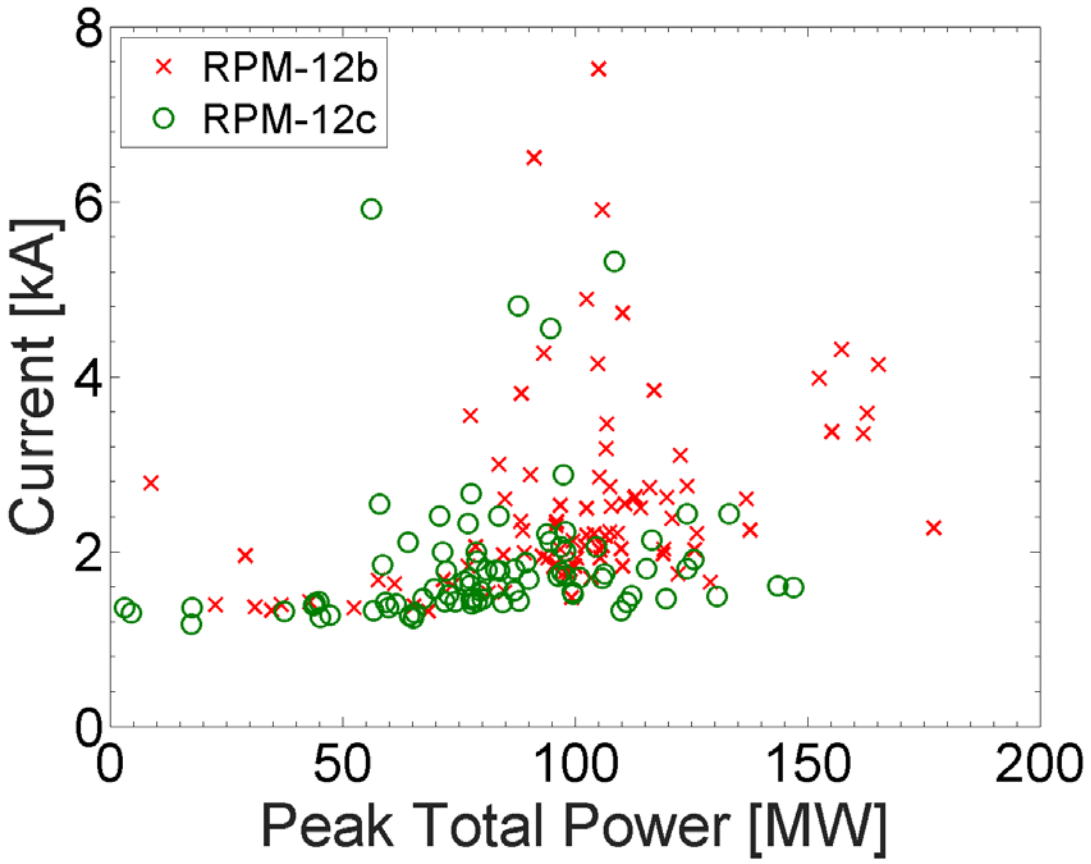

Figure 6: The 3D Printed Anodes were Subjected to Substantial Anode Current and Produced Peak Total Power up to 170 MW without Sustaining any Observable Damage or Reduction in Performance. It Should be Noted that this is the Peak Anode Current, not the Current at Peak Power

Both 3D printed anodes were tested for over 100 shots, experiencing currents of up to 8 kA, peak microwave power generation up to 170 MW and voltage pulses over -300 kV and 500 ns in duration. The RPM-12b was visually inspected after 50 and 100 shots, with no discernable operationally-induced damage. The RPM-12c was inspected after 100 shots and also appeared completely unchanged. Upon conclusion of all 200 shots, it was evident that a small amount of copper had deposited back onto the cathode, as it had taken on a faint orange sheen. It should be noted that neither anode was subjected to any runaway current events, which typically induce notable damage on our solid aluminum anodes. More rigorous durability studies (1000s of shots and material analysis) are planned for future work.

Due to non-uniform electroplating, the surfaces of the RPM-12b were not completely flat, leading to gaps where the anode and recirculating bend sections were bolted together (Figure 7a). These gaps caused poor electrical contact and minor arcing between the anode sections. Not all interfaces had visual evidence of arcing and Figure 7b shows the most prominent example. Future 3D printed structures will need to consider this aspect of electroplating and either

eliminate sections where electrical contact is a concern, or install the appropriate RF gasket material.

a)  b) 

Figure 7: Uneven Electroplating Leads to Poor Electrical Contact at Unions (a), Resulting in Arcing between the Parts during Operation (b)

No damage to the plastic substrate is expected, as the electrons should not penetrate either copper coating. Assuming a 300 keV maximum energy when the electrons strike the anode (in reality it will likely be much smaller, as the electrons give up some of their energy to the RF wave), the average path length traveled within copper, based on a continuous slowing down approximation (CSDA) is 140 μm [14]. The average penetration distance along the angle of impact, however, is only 45 μm [15]. Even in the case of an optimal perpendicular impact at full beam energy, the electrons will not penetrate either copping coating, whose thicknesses are over 200 μm.

4.4 Outgassing

Outgassing is one of the primary concerns for 3D printed structures. For our experimental setup, the base vacuum chamber pressure was consistently at $9x10^{-6}$ torr, regardless of which anode was in the chamber. For ultra-high vacuum conditions, where a bake-out is required, the outgassing and robustness of the 3D printed anodes would likely be more of a problem.

We first obtained a baseline measurement using the RPM-12a, noting a pre-shot vacuum composition of primarily N_2 and H_2O, as shown in the top half of Table 2. This is likely a result of a small vacuum leak at the microwave output windows. The RPM-12b had similarly high N_2 and H_2O levels, but substantially higher He. This was a result of the chamber being under vacuum for a longer period before beginning the shot series. Fifteen shots were conducted the

first day, the chamber was kept under vacuum and 40 more shots were conducted the following day. As the table shows, the He fraction continues to climb as high vacuum is maintained, eventually becoming the dominant component. In our system, this is likely the result of the higher He diffusion rate through rubber o-rings, its lower pumping speed within the cryopump and possibly saturation of the charcoal arrays within the pump [16]. After the second day of testing the RPM-12b, we opened the chamber to atmosphere to inspect the structure for any damage. No changes were observed and we finished the shot series the following day. Consequently, the He fraction decreased substantially. The chamber conditions before the third day are the most comparable to what was measured for the RPM-12a & c, as in all three cases the chamber had been pumped by a cryopump for roughly 24 hours. Comparing these three items in the table, we see comparable initial conditions.

Beyond the passive outgassing, we used the RGA to investigate the gas released during each microwave pulse. This was accomplished by subtracting a background histogram taken immediately before the shot from the histogram taken immediately after the shot. We initially expected we might see a "signature" gas for the 3D printed structures, which would appear only in their histograms, or in a larger quantity, but the observed post-shot outgassing was consistent for all three anodes, as shown in bottom half of Table 2. As expected, the primary constituent was H_2, with CO and CO_2 also contributing significant fractions. Compared to similar work in this area [17-18], the relative fraction of water vapor was unusually low, possibly due to the lack of a fast gate valve. The H_2 fraction is likely slightly overestimated, due to the way the RGA generates the histogram. We captured the histograms immediately after the shot, but the entire sweep from 1 to 50 amu still takes 1-2 seconds and starts at 1 amu. Consequently, the H_2 contribution is measured sooner, before the cryopump has reduced the inventory of all gases. Due to the small size of our chamber and the high pumping speed of the cryopump, the vacuum pressure decreases rapidly in the first 1 to 2 seconds. Attempts to reduce the pumping speed for better statistics resulted in unacceptably high base pressures, beyond what the RGA could reliably measure.

Table 2: Gas Inventories before each Shot Series Primarily Consisted of N_2 and H_2O, Irrespective of the Anode Material. Post-Shot Outgassing was also Similar for All Three Anodes; H_2 was the Primary Constituent, with CO and CO_2, also Consistently Contributing

Pre-Shot Conditions	**% CO_2**	**% CO**	**% He**	**% H_2**	**% N_2**	**% O_2**	**% H_2O**
RPM-12a	2	3	5	11	42	7	26
RPM-12b (1st day)	1	0	25	6	38	6	26
RPM-12b (2nd day)	1	0	35	4	35	5	20
RPM-12b (3rd day)	2	0	10	6	39	7	37
RPM-12c	2	3	5	11	44	8	27
Post-Shot Conditions							
RPM-12a	10	23	0	60	0	2	5
RPM-12b	11	25	0	60	0	0	4
RPM-12c	5	18	0	69	0	1	5

Due to the time required to complete a histogram sweep, we also monitored a single gas (CO_2) pressure as a function of time for all 3 anodes (Figure 8). The RGA can make this measurement at about 4 Hz, so we are able to more reliably capture the relative partial pressure of that gas. The RPM-12a had an average post-shot partial pressure of 1.48 x 10^{-4} torr, whereas the RPM-12b & c averaged 1.95 x 10^{-4} torr and 1.81 x 10^{-4} torr, respectively. As Figure 8 shows, the majority of shots registered just under 1 x 10^{-4} torr for each anode, but the 3D printed anodes had a larger percentage of high pressure events, saturating the RGA at 8.5 x 10^{-4} torr. We speculate that these events were due to pockets of gas being released as the beam impacts the anode.

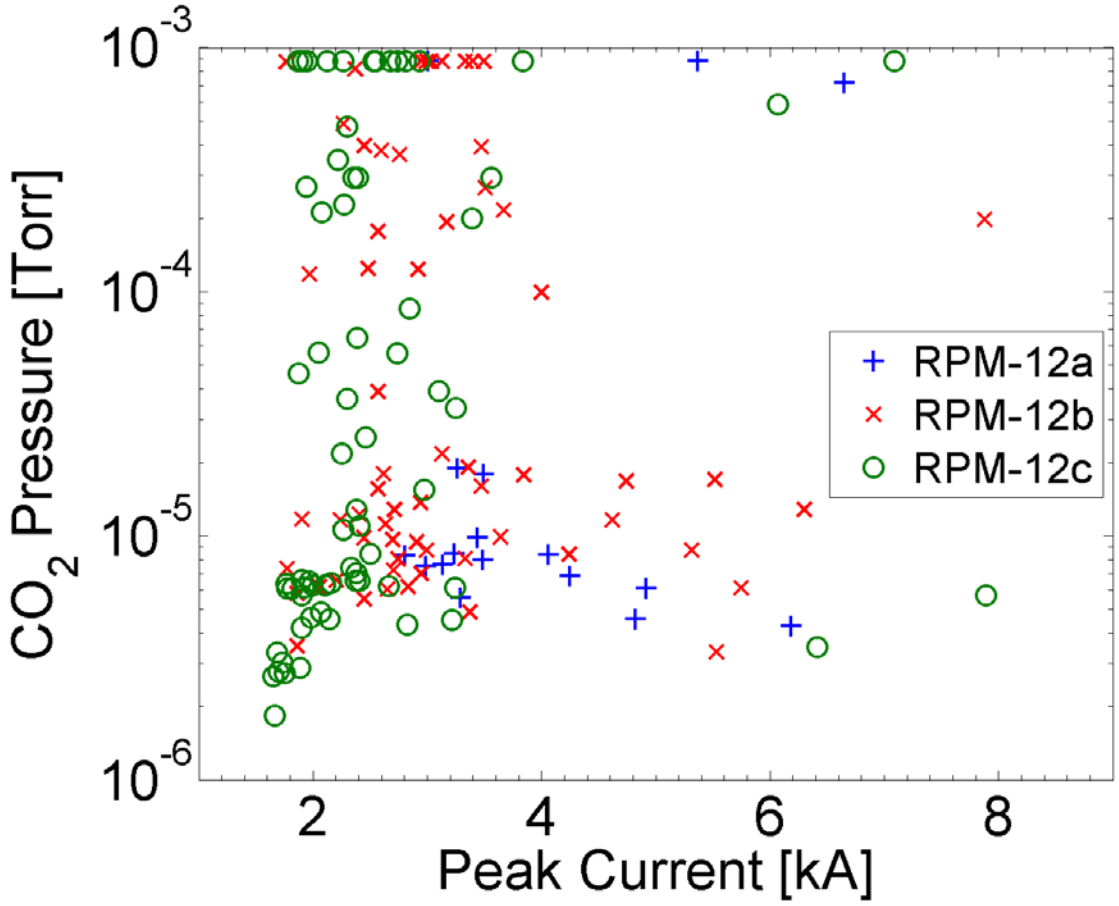

Figure 8: Partial Pressure of CO_2 within the Chamber Immediately Following Each Shot, Measured using the Pressure vs Time Mode of the RGA at 4 Hz. All Three Anodes Exhibited an Average Post-Shot Peak Pressure between 100 and 200 µtorr. The 3D printed Anodes had a Larger Percentage of High Pressure Events, Saturating the RGA at 8.5x10^{-4} torr

4.5 Long-Term Durability

As noted previously, ~100 shots per anode are not enough to establish the long term reliability of this manufacturing process. To further research the feasibility of these 3D printed structures in HPM devices, a repetitively pulsed experimental setup was designed and constructed. This setup, shown in Figure 9, is driven by a compact Marx generator (APELC MG-15-3C-940PF), capable of 300 kV, 30 ns pulses into a 50 Ω load. This generator can be fired at 10 Hz,

accumulating thousands of shots in a day. The voltage at the output of the generator is monitored with an imbedded D-dot probe, while the current is measured by a small Rogowski coil.

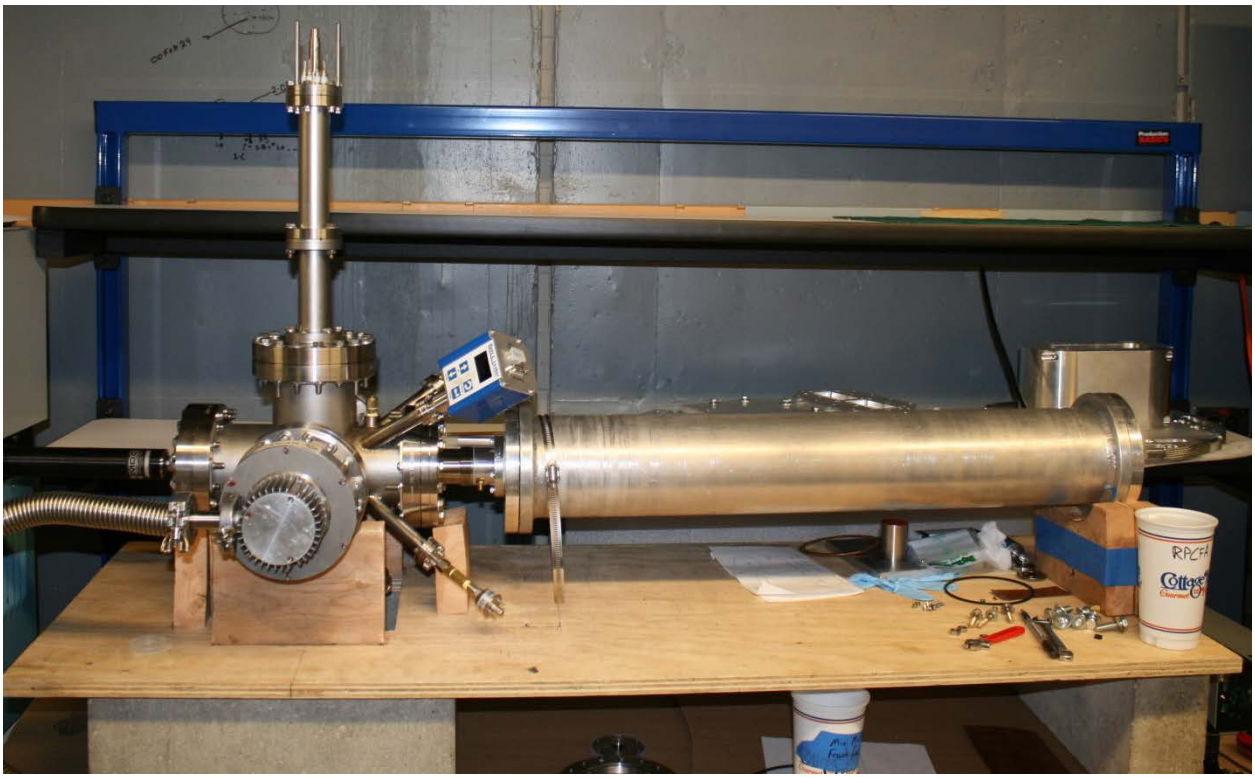

Figure 9: Test Chamber and Compact Marx Generator

The chamber is outfitted with a turbo pump backed by an oil-vane roughing pump and achieves pressures of 1x10-6 torr, as measured by the digital ion gauge in the figure. Also shown are a translational stage (left) for adjusting gap distance and a RGA (top) for monitoring gas species liberated during testing. The RGA electronics were removed for this photo, leaving only the measurement head and connection pins. A viewport is located on the back-side of the chamber, to provide imaging access during testing. The 3D printed anode and carbon cathode can be seen through the sample-loading port in Figure 10. In this photo, the Marx generator has been removed to rotate the test chamber, leaving only the insulating HV feedthrough.

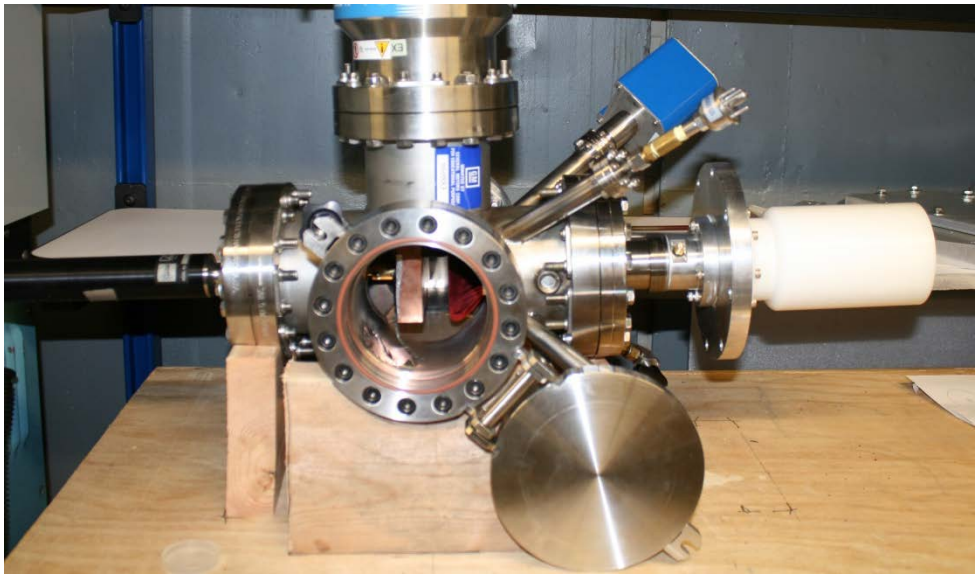

Figure 10: Test Chamber with RPM-12b Sample and Velvet Cathode

Due to vacuum system problems (now solved) and power supply problems (currently being resolved), no test data is available yet.

5.0 CONCLUSIONS

This work demonstrates that additively manufactured materials have promising potential applications in HPM. Despite being subjected to highly energetic electron beams, the anodes displayed no visible damage and no deleterious effects on performance. By all indications in this limited study, they were acceptable replacements for a solid metal anode block, allowing the relativistic planar magnetron to produce microwave pulses in excess of 150 MW, comparable with past results. Outgassing constituents from the additively manufactured structures were not substantially different from the aluminum control case, though they did exhibit slightly higher average post-shot vacuum pressures. Furthermore, the plastic anodes exhibited a higher incidence of large increases in gas pressure during the microwave pulse. In these instances, the gas pressure briefly increased beyond what the RGA could reliably measure. For the film thickness and beam energies tested, electron penetration into the plastic structure is not a concern, with thermal effects expected to be the dominant damage mechanism. Given the short timescales and low repetition rate of this work, significant thermal effects were not encountered, but are an important component of continued work in this area. The ~100 shots presented here demonstrate short-term durability, while the repetitively pulsed data will soon reveal longer-term performance.

6.0 REFERENCES

[1] R. J. Barker, J. H. Booske, N. C. Luhmann, Jr., G. S. Nusinovich, “Modern Microwave and Millimeter-wave Power Electronics,” John Wiley & Sons, Inc. (Hoboken, NJ, USA, 2005).

[2] J. Benford, J. A. Swegle, E. Schamiloglu, “High Power Microwaves,” Third Edition, CRC Press (Boca Raton, FL, USA, 2016).

[3] J. C. Whitaker, “Power Vacuum Tubes Handbook”, Second Edition, CRC Press (New York, NY, USA, 1999).

[4] X. Ge, J. Zhang, H. Zhong, and B. Qian, “A compact relativistic backward-wave oscillator with metallized plastic components,” Appl. Phys. Lett. 105, 123501 (2014).

[5] A. Palevsky and G. Bekefi, “Microwave emission from pulsed, relativistic E-beam diodes. II. The multiresonator magnetron,” Phys. Fluids, vol. 22, no. 5, pp. 986–996, May 1979.

[6] M. R. Lopez, R. M. Gilgenbach, M. C. Jones,W. M. White, D.W. Jordan, M. D. Johnston, T. S. Strickler, V. B. Neculaes, Y. Y. Lau, T. A. Spencer, M. D. Haworth, K. L. Cartwright, P. J. Mardahl, J. W. Luginsland, and D. Price, “Relativistic magnetron driven by a microsecond E-beam accelerator with a ceramic insulator,” IEEE Trans. Plasma Sci., vol. 32, no. 3, pp. 1171–1180 (2004).

[7] R. M. Gilgenbach, Y. Y. Lau, D. M. French, B. W. Hoff, J. Luginsland, and M. Franzi, “Crossed field device,” U.S. Patent US 8 841 867B2, Sep. 23, 2014.

[8] R. M. Gilgenbach, Y. Y. Lau, d. M. French, B. W. Hoff, M. Franzi, and J. Luginsland, “Recirculating Planar Magnetrons for High-Power High-Frequency Radiation Generation,” IEEE Trans. Plasma Sci., Vol 39, No. 4, pp. 980 - 987 (2011).

[9] M. A. Franzi, R. M. Gilgenbach, B. W. Hoff, D. A. Chalenski, D. Simon, Y. Y. Lau, and J. Luginsland, “Recirculating-Planar-Magnetron Simulations and Experiment,” IEEE Trans. Plasma Sci., Vol 41, No. 4, pp. 639 - 645 (2014).

[10] M. A. Franzi, G. B. Greening, N. M. Jordan, R. M. Gilgenbach, D. H. Simon, Y. Y. Lau, B. W. Hoff, and J. Luginsland, “Microwave Power and Phase Measurements on a Recirculating Planar Magnetron,” IEEE Trans. Plasma Sci., Vol. 43, No. 5, pp. 1675 – 1682 (2015).

[11] Dsm.com, "Somos® WaterShed XC 11122: The difference is clear", 2016. [Online]. Available: http://www.dsm.com/products/somos/en_US/offerings/offerings-somos-water-shed.html. [Accessed: 03- Jan- 2016].

[12] Fini-finish.com, "fini finish metal finishing | chrome plating | rapid prototype | restoration", 2016. [Online]. Available: http://www.fini-finish.com/. [Accessed: 03- Jan- 2016].

[13] M. Franzi, R. Gilgenbach, Y. Y. Lau, B. Hoff, G. Greening, and P. Zhang, “Passive mode control in the recirculating planar magnetron,” Physics of Plasmas, vol. 20, no. 3, p. 033108, 2013.

[14] Berger, M.J., Coursey, J.S., Zucker, M.A., and Chang, J. (2005), ESTAR, PSTAR, and ASTAR: Computer Programs for Calculating Stopping-Power and Range Tables for Electrons, Protons, and Helium Ions (version 1.2.3). [Online] Available: http://physics.nist.gov/Star [2016, Jan 8]. National Institute of Standards and Technology, Gaithersburg, MD.

[15] V. Lazurik, V. Moskvin and T. Tabata, "Average depths of electron penetration: use as characteristic depths of exposure", IEEE Trans. Nucl. Sci., vol. 45, no. 3, pp. 626-631, 1998.

[16] D. Hoffman, B. Singh and J. Thomas, *Handbook of vacuum science and technology*. San Diego, CA: Academic Press, 1998.

[17] M. Cuneo, "The effect of electrode contamination, cleaning and conditioning on high-energy pulsed-power device performance", IEEE Transactions on Dielectrics and Electrical Insulation, vol. 6, no. 4, pp. 469-485, 1999.

[18] R. Gilgenbach, J. Hochman, R. Jaynes, W. Cohen, J. Rintamaki, C. Peters, D. Vollers, Y. Lau and T. Spencer, "Optical spectroscopy of plasma in high power microwave pulse shortening experiments driven by a μs e-beam", IEEE Trans. Plasma Sci., vol. 26, no. 3, pp. 282-289, 1998.

LIST OF SYMBOLS, ABBREVIATIONS, AND ACRONYMS

3D	Three dimensional
AFOSR	Air Force Office of Scientific Research
AFRL	Air Force Research Laboratory
AK	Anode-Cathode
CSDA	Continuous slowing down approximation
FFT	Fast Fourier Transform
HPM	High Power Microwaves
MCC	Mode Control Cathode
MELBA-C	Michigan Electron Long Beam Accelerator with a ceramic insulator
RBWO	Relativistic Backward Wave Oscillator
RGA	Residual Gas Analyzer
RF	Radio Frequency
RPM	Recirculating Planar Magnetron
SLA	Stereolithography
SWS	Slow Wave Structure

DISTRIBUTION LIST

DTIC/OCP
8725 John J. Kingman Rd, Suite 0944
Ft Belvoir, VA 22060-6218 1 cy

AFRL/RVIL
Kirtland AFB, NM 87117-5776 1 cy

Official Record Copy
AFRL/RDHP/Brad Hoff 1 cy